Effects of synthesis conditions on the structural features and methane adsorption properties of single-walled carbon nanohorns prepared by a gas-injected arc-in-water method

Noriaki Sano,[a] Yoshihiro Akita, and Hajime Tamon
Department of Chemical Engineering, Kyoto University, Kyoto 615-8510, Japan

(Received 18 January 2011; accepted 14 May 2011; published online 21 June 2011)

Single-walled carbon nanohorns (SWCNHs) can be easily synthesized via a gas-injected arc-in-water method that is considered to be a cost-effective technique. The electrode configuration and duration of arc discharge were modified in order to enhance the yield and methane-adsorption properties of SWCNHs. As a result, the yield of the SWCNHs was significantly increased by increasing the discharge time and the size of the cathode. Using these modified conditions, the horn units in the SWCNH aggregates increased in size, and the thermal stability of SWCNHs in an oxidative environment increased accordingly. *Ab initio* molecular orbital calculations were used to explain the trend in the thermal stability. When the conventional conditions were applied, a burn-off of about 40% was necessary in order to achieve the maximum specific surface area and micropore volume. Remarkably, by enlarging the cathode size, the burn-off can be reduced by almost half to achieve the enhanced micropore volume. As a result, SWCNHs obtained using the modified conditions adsorbed a larger amount of methane than did SWCNHs obtained from the conventional synthetic conditions. The effect of a mild oxidation treatment on SWCNHs on their methane adsorption suggested that SWCNHs with micropores would be more flexible than pristine SWCNHs. This tendency was elucidated using a molecular mechanics calculation. © *2011 American Institute of Physics*.
[doi:10.1063/1.3600236]

I. INTRODUCTION

Nanotube-family carbon materials, including multi-walled carbon nanotubes (MWCNTs),[1] single-walled carbon nanotubes,[2] single-walled carbon nanohorns (SWCNHs),[3] carbon nanoonions,[4] and so forth, have received intense attention because of their unique structures and physical properties.[5–12] As a result, the synthesis and applications of these materials have been highly developed.[13–19] Among these materials, SWCNHs are considered as promising materials for many applications such as drug delivery,[20] energy applications,[21–23] gas adsorptions,[23–26] etc. Within the literature concerning their energy applications based on adsorption, it was reported that SWCNHs are promising materials for methane storage.[23,24]

SWCNHs can be prepared via several methods using high power lasers or arc discharge.[3,18,19,27–34] In this study, the gas-injected arc-in-water (GI-AIW) method[18,27,35] was adopted, as it is considered as a low-cost technique among the methods that yield SWCNHs. Here, the conditions of the synthesis using the GI-AIW method were modified in order to improve the production yield and methane-adsorption ability of SWCNHs. The influence of the synthetic conditions on the structures and thermal stabilities of SWCNHs was investigated.

In order to improve the methane-adsorption properties of SWCNHs, the SWCNHs were heat treated in an oxidizing gas environment at an appropriate temperature for a specific time so as to effectively open micropores on their surfaces.[24–26] Through this heat treatment, the purity of the SWCNHs was expected to be improved due to the combustion of amorphous carbon impurities.[25] In addition, mechanical compression of the SWCNHs effectively increased the amount of methane adsorbed per apparent volume of SWCNHs.[24] Although the amount of gas molecules adsorbed per mass of adsorbent is usually used to indicate adsorption properties, it is also an important parameter for the practical design of gas storage devices for industrial applications. In previous reports,[24,26] the influences of the extent of oxidation and compression on methane adsorption were not investigated; these influences were closely investigated in the present study.

II. EXPERIMENTAL DETAILS

A. Synthesis of SWCNHs

Details of the GI-AIW method used in this study are described elsewhere.[18,27,35] In this article, only a depiction of the electrode dimensions is shown (Fig. 1), and the details of the apparatus can be obtained from the cited references. A graphite rod (diameter = 12 mm, length = 5 cm) with a hole (diameter = 8 mm, depth = 25 mm) on the bottom along its axis was used as a cathode, and another graphite rod (diameter = 3 mm) was used as an anode. These dimensions are referred to as the conventional conditions that were adopted in previous studies. In order to investigate the effects of the size of the cathode hole, a cathode with a larger hole diameter of 12 mm was prepared. The electrodes in the

[a]Author to whom correspondence should be addressed. Electronic mail: sano@cheme.kyoto-u.ac.jp.

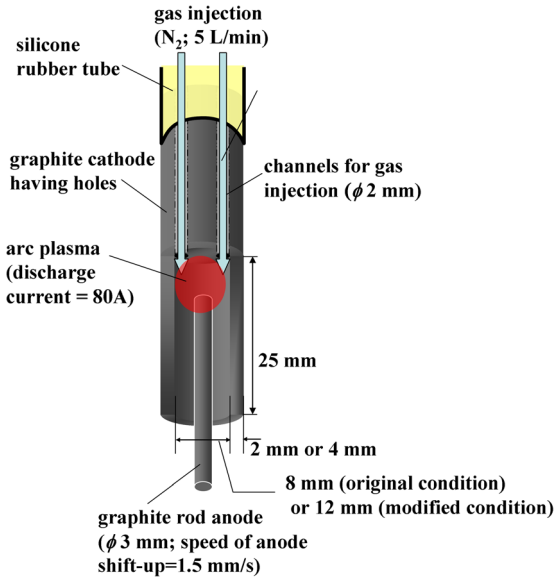

FIG. 1. (Color online) Dimensions of graphite electrodes used in the present study.

GI-AIW method were submerged in water. On the top of the cathode, two narrow channels were drilled in order to introduce N_2 at a rate of 5 L min^{-1}. The arc discharge was generated inside the cathode hole, and carbon vapor emitted by the vaporization of the graphite anode was carried to the water by N_2 flow. In the experiments referred to as the conventional synthetic conditions, the anode was moved upward at a rate of 1.5 mm s^{-1} using a motor-driven slider to generate arc discharge at 80 A for 18 s. During the arc discharge, only the anode was consumed. When the synthetic conditions were modified, the arc discharge time was increased while maintaining the anode's ascending speed. In this reaction system, the vaporization of the graphite anode by hot arc plasma (at approximately 5000 K) followed by a quick transfer to water causes a high quenching rate of the carbon vapor (2×10^6 K s^{-1} level),[35] resulting in the formation of SWCNHs via a self-transforming mechanism.[36] The SWCNHs were collected in a powdery form that floated on the water's surface and which was separated from bulky deposits containing MWCNTs, which settled to the bottom of the container. The as-grown SWCNHs were dried at 50 °C for one day in ambient air, followed by drying *in vacuo* prior to post-treatments (mild oxidation and compression) and analyses.

B. Oxidation and compression on SWCNHs

A mild oxidizing treatment of the as-grown SWCNHs was conducted by heating the SWCNHs at 773 K in an oxidative gas environment using a cylindrical electric furnace. The powdery SWCNHs were placed on a ceramic boat in a quartz tube (inner diameter = 33 mm) that was set in the furnace with an O_2 flow at a rate of 500 cm^{-3} min^{-1}. Otherwise, the heat treatment was carried out in ambient air in an open-ended quartz tube. The weight change of the SWCNHs caused by this oxidation treatment was measured; burn-off is defined as the ratio of the weight change to the initial weight of the SWCNHs. The time for this heat treatment was varied between 10 and 60 min in order to change the burn-off.

The powdery SWCNHs were also compressed at pressures of up to 18 MPa using a mold so as to form a pellet. The diameter of the pellet was 8.4 mm, and its thickness was in the range of 2 to 8 mm, depending on the compression pressure. This pellet was compressed twice in order to improve its packing density.

C. Characterization of SWCNHs and methane adsorption measurement

The structures of the SWCNHs were observed via transmission electron microscopy (TEM) (JEOL, JEM2010). The Brunauer-Emmett-Teller (BET) surface area of the SWCNHs was determined via the adsorption of N_2 at 77 K using an automatic system (BEL Japan, Bel-Mini). In this article, the definitions of mesopores and micropores proposed by the International Union of Pure and Applied Chemists were adopted. The pore size distribution was analyzed using the Dollimore–Heal method[37] and the Horvath–Kawazoe method[38] for the mesopores and the micropores, respectively. The micropore volume was determined using the t-plot method.[39] Methane adsorption on the SWCNHs was measured using a magnetic suspension balance (Rubotherm, MSB-MT-CP-HP-SP) in a range of methane pressures up to 4 MPa; this measurement was conducted at room temperature. In addition, thermal gravimetric (TG) analysis and differential thermal analysis (DTA) were performed using a TG/DTA analyzer (Shimadzu, TGA-50) in order to evaluate the thermal stability of the SWCNHs in an oxidative environment. The temperature elevation rate in the TG/DTA analyses was 10 °C min^{-1}.

III. RESULTS AND DISCUSSION

A. Influence of synthetic-condition modifications on SWCNH yield

Figure 2 shows photographic images of the graphite anodes that were used in the GI-AIW method. When a cathode-hole diameter of 8 mm was used, the consumption of the anode during arc discharge was not perfectly localized at the tip; instead a relatively large area of the anode was consumed, as shown in the upper image (Fig. 2). This indicates that the arc plasma can expand in the narrow zone between the electrodes inside the cathode hole. Under such conditions, the resident time of the carbon vapor generated by the evaporation of the graphite anode in the inter-electrode space cannot be uniform. Therefore, some of the carbon vapor will be expelled into the water before being transformed into SWCNHs and will react with H_2O to form H_2 and CO.[27] This reaction would cause a significant decrease of the yield of SWCNHs. The expansion of the cathode-hole diameter to 12 mm effectively minimized this effect. After this modification, the area of the graphite anode that was consumed by the arc discharge became localized in a narrower range around its tip, as shown in the lower image (Fig. 2).

Figure 3 shows the influences of the diameter of the cathode hole and the arc discharge time. The yield of SWCNHs

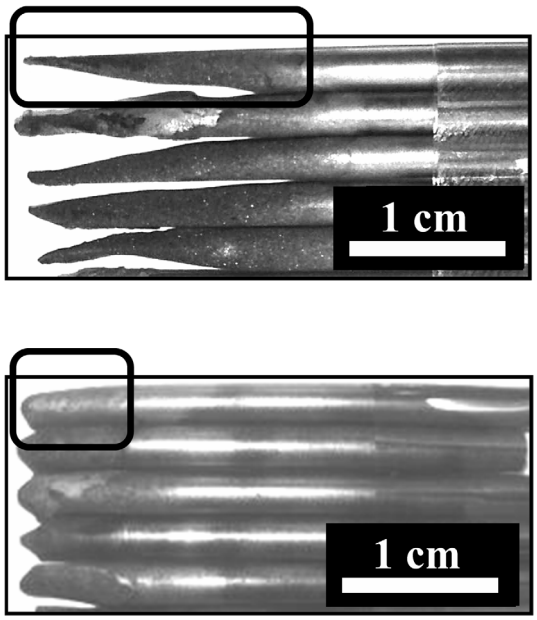

FIG. 2. Photographs of graphite anodes consumed by arc discharge. The upper image corresponds to the conventional condition (cathode hole diameter = 8 mm) and the lower image corresponds to the modified condition (cathode hole diameter = 12 mm). The areas outlined by squares show the consumed parts.

observably increased when the cathode-hole diameter was increased from 8 mm to 12 mm. This increase of the yield of SWCNHs is due to the change of the reaction field, which caused the resident time of the carbon vapor to become more uniform and reduced the loss of carbon vapor caused by its reaction with H_2O.

Furthermore, Fig. 3 suggests that the yield of SWCNHs increased significantly with an increase in the arc discharge time. This tendency is consistent with previously reported information about arc discharge modes (continuous and discrete arc modes).[40] According to this report, the temperature of the arc discharge plasma is initially about 4650 K and gradually increases up to 5100 K during arc discharge in the time range observed here. With respect to the effect of temperature on the yield of SWCNHs, information concerning the temperature dependency of the plasma density in the carbon arc has been reported[41]; the C^+ density increases from

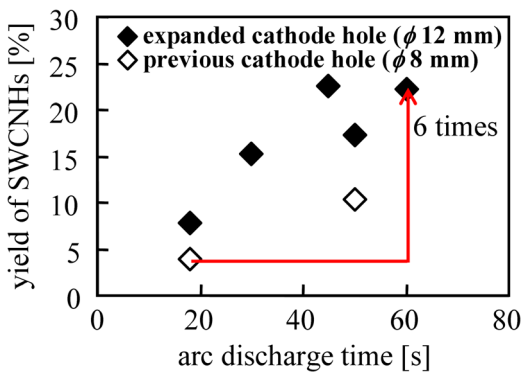

FIG. 3. (Color online) Yield of as-grown SWCNHs synthesized using various synthetic conditions. The conventional condition includes an arc discharge time of 18 s with a cathode hole diameter of 8 mm.

about 1×10^{13} to 5×10^{13} cm^{-3}, and the C density increases from about 2×10^{17} to 4×10^{17} cm^{-3} upon a temperature elevation from 4500 K to 5000 K. A similar composition change would occur in our system. When the C density increases, the condensation of carbon vapor will be accelerated due to an increase in the collision frequency of C radicals forming carbon droplets. The carbon droplets are then converted into SWCNHs.[42] Therefore, the yield of SWCNHs should increase when the formation of carbon droplets is accelerated by higher temperatures and a longer arc discharge time. Consequently, the yield of SWCNHs using the modified conditions was almost 6 times greater than that using the conventional conditions.

One might wonder whether the final yield of ~23% is high, given that the yield of soot containing SWCNHs produced via the method of laser ablation was reportedly 75%.[3] The yield obtained using the GI-AIW method is still lower than that obtained from such laser ablation methods. Nevertheless, the capital costs and running costs of any high power laser system must be extremely high as compared with those of the arc discharge system. Thus, the yield of 23% can be considered to be high with respect to the cost-effectiveness of the technique. Additionally, useful byproducts, including MWCNTs and H_2, can be obtained separately using the GI-AIW method.[18,27]

B. Influence of synthetic condition modifications on SWCNH structures

Figure 4 shows two typical TEM images of SWCNHs produced using the conventional conditions (arc discharge time = 18 s) and the modified conditions (arc discharge time = 60 s). The SWCNHs produced with the conventional conditions, as shown in Fig. 4(a), had relatively small horns that could not be clearly resolved by low magnification observation. When the structures of these particles were closely observed, dense aggregations of small horns with diameters of 1 to 2 nm were seen, as shown in the close-up image. Below that image, a schematic image of the structure of such a horn aggregate is illustrated. In contrast to the SWCNHs shown in Fig. 4(a), the SWCNHs shown in Fig. 4(b) exhibit relatively large horns, which were clearly resolved even at low magnification. The particle marked by a square, b-1, was very similar to the ones synthesized via laser ablation, which tended to be directed along radial directions. Thus, many horns protruded, as shown in square b-2. In addition, the structures of the unidirectional aggregates of horns shown in square b-3 were seen in many places. When the arc discharge time was extended to 60 s, the structures shown in Fig. 4(b) significantly dominated the structures shown in Fig. 4(a).

The reason why the horns obtained with a longer arc discharge time tend to be larger than those obtained with a shorter arc discharge time has not yet been clarified. Nevertheless, molecular calculations that can verify the self-assembling mechanisms leading carbon to form curled graphene-wall junctions,[36] which can be considered as part of the structure of SWCNHs, are useful in elucidating the mechanism of SWCNH formation. Based on this result, it is hypothesized that graphene sheets, which appear on carbon droplets at

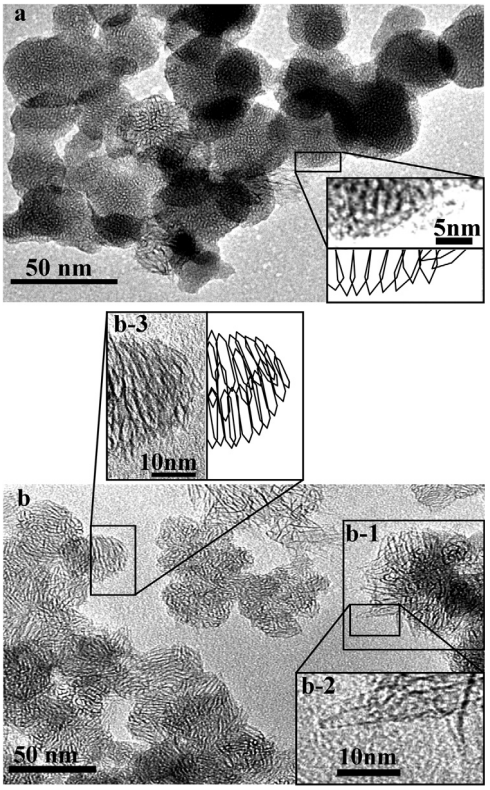

FIG. 4. TEM images of two typical structures of SWCNHs. The upper image (a) shows the main structure when an arc discharge time of 18 s and a cathode hole diameter of 8 mm were adopted. The lower image (b) shows the main structure when an arc discharge time of 60 s and a cathode hole diameter of 12 mm were adopted.

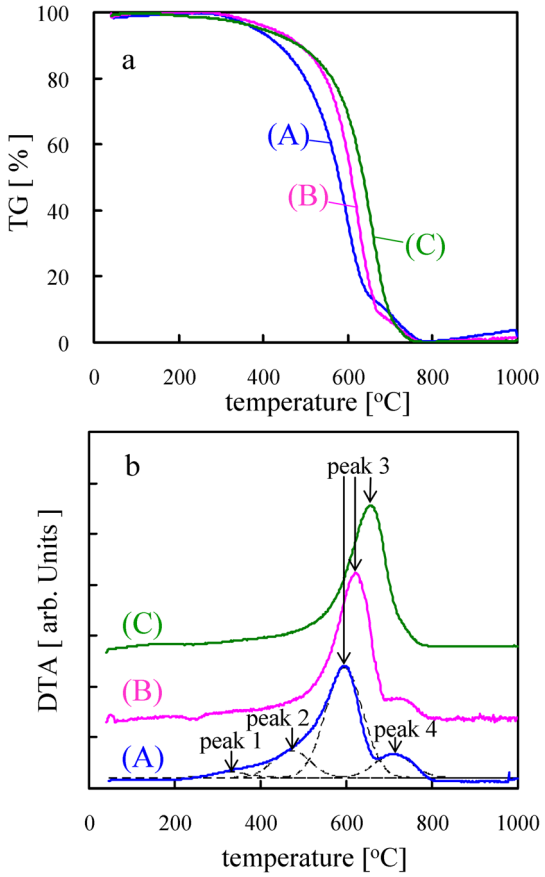

FIG. 5. (Color online) (a) TG and (b) DTA charts of SWCNHs synthesized using the conventional condition (A: arc discharge time = 18 s with a cathode hole diameter = 8 mm) and the modified conditions (B: arc discharge time = 50 s with a cathode hole diameter = 8 mm; C: arc discharge time = 60 s with a cathode hole diameter = 12 mm). The temperature elevation rate in the TG/DTA analyses was 10 °C min^{-1}.

high temperatures, can form horn structures when the sheet reaches the size range preferable for the formation of SWCNHs.[42] In order for this to be valid, relatively large horn structures require that the graphene sheets on the carbon droplets must grow to a large size while the graphene sheets are curled and merged. Therefore, we propose that the growth of large graphene sheets requires high temperatures that are held for a sufficient time to complete the formation of the SWCNH structures. When the temperature of the reaction field is not high enough, the time for which the graphene sheets can stay in the high temperature zone becomes shorter, and the graphene sheets will close and make small horn shapes before the graphene sheets grow very large.

C. Thermal stabilities of SWCNHs in oxidative environments

The thermal stabilities of the as-grown SWCNHs in oxidative environments were evaluated based on the TG/DTA analyses. These analyses reflect the structures and purity of the carbonaceous components in the products.[25] Fig. 5 shows the results of TG/DTA on SWCNHs synthesized using the conventional condition (arc discharge time = 18 s, cathode-hole diameter = 8 mm) and the modified conditions with extended arc discharge times and a larger cathode-hole diameter. In the TG charts, it can be seen that the weights of the samples gradually decrease as the temperature increases from 300 °C with increasing slopes, and there is a temperature at which a clear change is evident in the slope above 600 °C. This slope change indicates a mixture of different carbonaceous structures. The DTA charts more clearly show the differences between the samples. In the DTA analysis, four peaks were included in one chart. According to the literature,[25] peaks 1, 2, 3, and 4 in Fig. 5(b) should correspond to the combustion peaks of amorphous carbon, defective carbon with non-six-membered rings, tubular graphene, and graphitic carbon impurities, respectively. The tubular graphene, which is indicated by peak 3, represents the tubular horn units that are the main structures in SWCNHs.

In this figure, it was remarkable that peak 3 became more prominent when the condition modifications were implemented. In particular, curve (C), corresponding to the modified conditions with an arc discharge time of 60 s and a cathode-hole diameter of 12 mm, exhibited only peak 3 as a significant peak; the other peaks became almost negligible. This result suggests that the purity of SWCNHs produced via the GI-AIW method was significantly improved by the condition modifications.

It was also remarkable that the position of peak 3, which represents the horn units, tended to shift to a high temperature range when the synthetic conditions were modified. This shift is likely related to the structural changes in the SWCNHs. In order to elucidate the influence of the average horn size on the DTA charts, the heat of reaction required to

open a micropore on a model SWCNH was calculated via *ab initio* molecular orbital calculations using the LANG2MB basis set.[43] It should be noted that this basis set is not for calculating absolute values with high accuracy, but rather for discussions based on qualitative comparison. This calculation was conducted using GAUSSIAN 03 W commercial software (Gaussian Inc.).[44] The SWCNH model with 78 atoms that was used in this calculation is shown in Fig. 6. In this calculation, various locations of the C atoms were targeted for oxidation in order to make one-atom pores; therefore, an influence of the SWCNH diameter at the location of the removed C atom was observed. The reaction scheme used to calculate the heat of reaction for opening a one-atom pore is as follows:

$$\mathrm{HRN} + 1/2\ \mathrm{O_2} \rightarrow \mathrm{d\text{-}HRN} + \mathrm{CO_2}, \quad (1)$$

where HRN and d-HRN demote the pristine SWCNH model and its defective structure, respectively. The structure of d-HRN is obtained by removing one of the C atoms from a numbered location on the HRN structure shown in Fig. 6. The heats of reaction, as determined by Eq. (1), that were obtained from the various locations of the removed C atoms are plotted against the corresponding horn diameter in Fig. 6. It is evident that the heat of reaction, which is the energy required to open a pore on a SWCNH, decreases with decreasing horn diameter. This means that it is easier to open a micropore at the narrower part of the SWCNH structure. This tendency is likely caused by the increase of the curvature of the horn surface at smaller diameters. Thus, because the combustion of SWCNHs occurred with the opening of micropores, peak 3 indicates that the combustion of the main SWCNH structure can occur in a milder environment when the average diameter of the horns is smaller. Therefore, the lower temperature of peak 3 in Fig. 5(b) likely corresponds with narrower SWCNH diameters. Therefore, the shift of peak 3 to a higher temperature when using the modified conditions suggests that the average horn diameter increased when the reaction conditions were modified. This tendency is consistent with the TEM observations shown in Fig. 4.

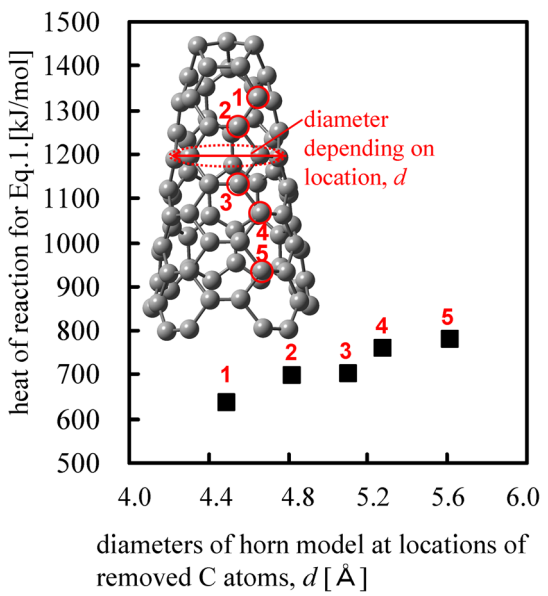

FIG. 6. (Color online) Influence of the location of the one-atom pore on the heat of reaction needed to open the pore on a SWCNH model calculated using Eq. (1). The number at each plot corresponds to the location of the removed C atom, as shown in the embedded SWCNH model.

D. Porous properties of SWCNHs and the effect of post-treatments

The BET surface area, S_{BET}, and the micropore volume, V_{micro}, of SWCNHs that were oxidized by heat treatment are shown in Fig. 7 as a function of the burn-off. An evaluation of the micropore volume is important because the adsorption of methane on SWCNHs should occur first on micropores that exist in the interstitial spaces between the tubular horns.[23] It is reported that when the concentration of methane increases in the interstitial spaces, adsorption in the internal spaces of tubular SWCNH structures can be enhanced by a unique mutual-enhancement effect.[23] In Fig. 7, the open symbols show the results from the SWCNHs synthesized using the conventional conditions (cathode-hole diameter = 8 mm), and the solid symbols show the results from those obtained using the modified conditions (cathode-hole diameter = 12 mm).

With a cathode-hole diameter of 8 mm, there was a clear optimal value of burn-off of approximately 40% needed to simultaneously maximize the S_{BET} and V_{micro} of the SWCNHs. The values of S_{BET} and V_{micro} of the SWCNHs oxidized by the optimized burn-off were 4.4 and 17.5 times larger, respectively, than those of the as-grown SWCNHs.

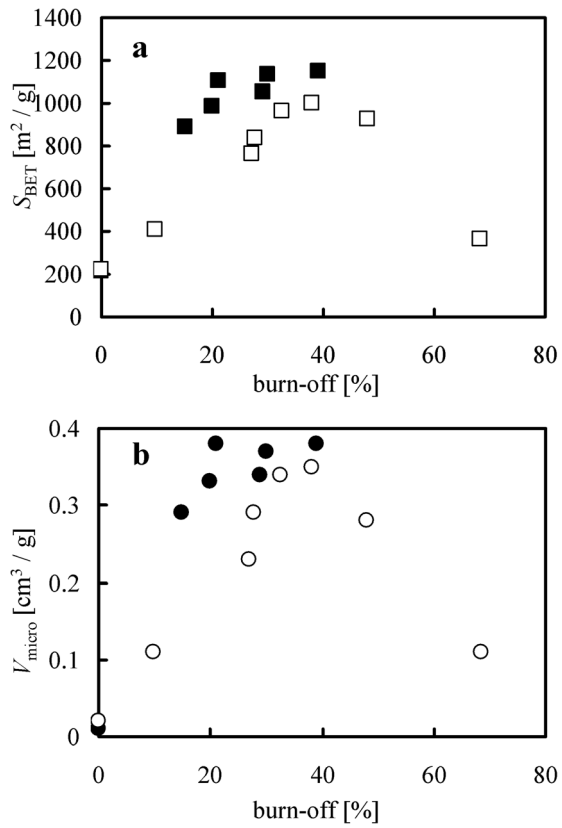

FIG. 7. Influence of burn-off on the (a) BET surface area and (b) micropore volume of SWCNHs. The open symbols correspond to the conventional conditions with an arc discharge time of 18 s and a cathode hole diameter of 8 mm. The solid symbols correspond to the modified conditions with an arc discharge time of 60 s and a cathode hole diameter of 12 mm.

The increase of S_{BET} and V_{micro} with increasing burn-off in the range lower than the optimized burn-off is caused by the opening of micropores on the SWCNHs. The opposite tendency in the range higher than the optimized burn-off is caused by the destruction of the horn structures of the SWCNHs. It was confirmed by TEM that only large graphite flakes remained after thorough oxidation by heat treatment.

In the case of a cathode-hole diameter of 12 mm, it is remarkable that the dependency of the burn-off on these porous properties was not significant in the burn-off range from 20% to 40%, suggesting that the ideal burn-off to achieve high methane adsorption on SWCNHs would be reduced by about half by the modification of the synthetic conditions. This difference relative to the values obtained with the conventional synthetic conditions is attributed to the reduction of impurities.

Figure 5 shows information about the inclusion of impurities. The DTA chart in Fig. 5(b) for the modified condition (C) did not exhibit the peaks corresponding to impurities (peaks 1, 2, and 4) that were clearly evident in the DTA results for the products from the conventional condition (A). In the case of the conventional condition, amorphous carbon and defective carbon should be combusted by oxidation treatment in the low burn-off range. Therefore, the increase of the BET surface area and micropore volume of the SWCNHs produced with the conventional conditions in the low burn-off range is likely due to the opening of micropores on the tubular walls of the SWCNHs combined with the combustion of these impurities. In contrast, the oxidation of the SWCNHs produced using the modified condition (C) would not include significant combustion of such impurities because of the high purity of the SWCNHs. Thus, the high BET surface area and micropore volume at a relatively low burn-off (20%) are realized via the opening of micropores without inhibition by impurities on the SWCNH surface. Additionally, the BET surface area and the micropore volume of SWCNHs from the modified condition did not increase when the burn-off increased from 20% to 39% due to a limited pore density (number of pores per surface area of SWCNHs). We propose that the pore density cannot increase above a certain limit, and further oxidation of the tubular horns would result in destruction of the horn structure.

The apparent density of the SWCNH bulk can be monotonically increased with compression pressure, as shown in Fig. 8. Figure 9(a) shows the pore size distribution in the micro- and mesopore ranges at varied compression pressures. As shown, the peak of the mesopore size distribution tended to shift to a smaller size range when the compression pressure increased. Note that the mesopores would exist in the spaces between the tubular horn structures and that the dominant spaces in the inner spaces of the tubular horns should be regarded as mesopores. Therefore, it is reasonable that these mesopores become smaller when the SWCNHs are packed more densely due to increased compression. In contrast, the micropore size distribution was independent of compression.

The micropore size distributions of the SWCNHs prepared under the modified synthetic conditions are shown in Fig. 9(b) in comparison with those of the SWCNHs obtained via the conventional synthetic condition. It was confirmed

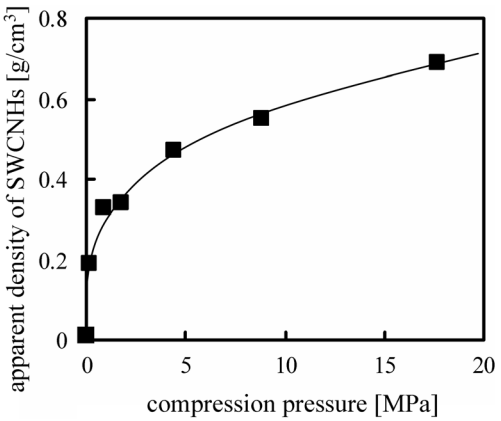

FIG. 8. Relation of compression pressure to the apparent density of SWCNH bulk. The sample was prepared using an oxidation treatment for a burn-off of 27% on SWCNHs obtained from a synthetic condition with an arc discharge time of 18 s and a cathode-hole diameter of 8 mm.

that the SWCNHs prepared using the modified conditions had larger micropore volumes, although the peak position did not change from that of the conventional condition.

E. Methane adsorption

Figure 10 shows the amount of methane adsorbed on the SWCNHs at elevated methane pressures. In this figure, the amount of methane adsorbed is shown in the unit of its STP volume (volume at 0 °C and 1 atm) per apparent volume of

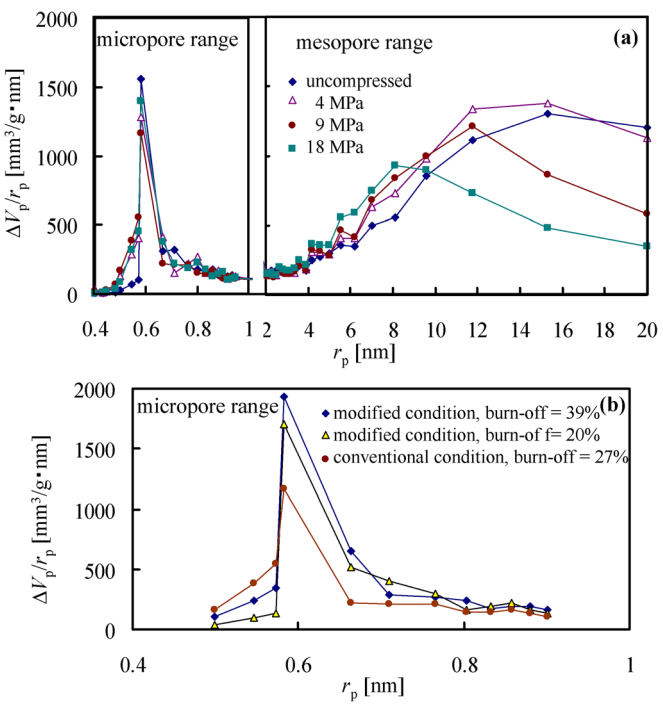

FIG. 9. (Color online) Diameter distributions of the micropore and mesopore ranges of SWCNHs prepared via oxidation treatment for a burn-off of 27% on SWCNHs obtained from the conventional synthesis condition with an arc discharge time of 18 s and a cathode hole diameter of 8 mm in the upper plots (a). The lower plots (b) show the diameter distributions of the micropores of SWCNHs prepared with both conventional conditions (arc discharge time = 18 s, cathode hole diameter = 8 mm, burn-off = 27%) and modified conditions (arc discharge time = 70 s, cathode hole diameter = 12 mm, burn-off = 20% and 39%).

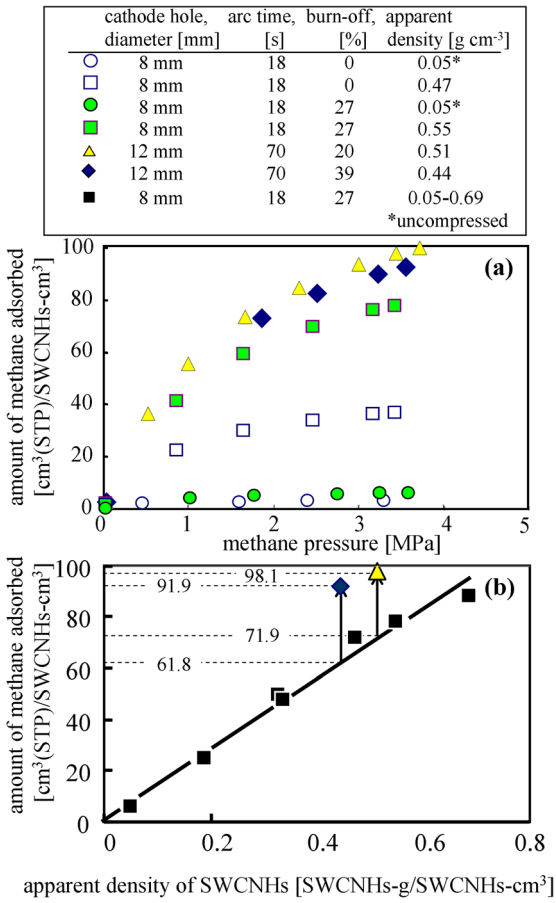

FIG. 10. (Color online) Amount of methane adsorbed on SWCNHs per apparent volume of SWCNH bulk. In the upper plots (a), one can compare the uncompressed (density = 0.05 g cm^{-3}) and compressed SWCNHs, as well as the oxidized and pristine (burn-off = 0%) SWCNHs. In the lower plots (b), one can observe the relation of the amount of methane adsorbed on SWCNHs to their apparent density, and the effect of the synthetic condition modifications on the SWCNHs.

SWCNH bulk. Figure 10(a) shows the amount of methane adsorbed per apparent volume of SWCNH bulk as a function of methane pressure. In the case of the conventional synthetic conditions (cathode-hole diameter = 8 mm; arc time = 18 s), the amount of methane adsorbed onto the SWCNHs can be compared between compressed and uncompressed SWCNHs, and between oxidized and non-oxidized SWCNHs. It can be readily observed that the amount of methane adsorbed per apparent volume of SWCNH bulk drastically increases with compression. This result can be reasonably understood because the apparent density of the SWCNH bulk is increased by compression, as mentioned in the previous section. Figure 10(b) reveals that the amount of methane adsorbed per apparent volume of SWCNH bulk increases linearly at a slope of 135 cm^3 g^{-1}; this value corresponds to the amount of methane adsorbed per mass of SWCNHs. This linearity suggests that the methane adsorbed per mass of SWCNHs is constant regardless of the apparent density of SWCNHs. Remember that the micropore size distribution is not dependent on the compression pressure, although the mesopore range is significantly affected. These results can be explained by the understanding that the adsorption of methane on the micropores should decisively dominate the total amount of the methane adsorbed on SWCNHs.

By comparing the methane adsorption on the oxidized SWCNHs to that on the pristine SWCNHs (burn-off = 0%), one can see that the oxidation of the SWCNHs significantly increased the amount of methane adsorbed per apparent volume of SWCNH bulk. The amount of methane adsorbed per apparent volume of oxidized SWCNHs was about 2 times larger than that of pristine SWCNHs.

The amount of methane adsorbed per mass of oxidized SWCNHs can be obtained as the amount of methane adsorbed per apparent volume multiplied by the apparent density. It was confirmed that the amount of methane adsorbed per mass of oxidized SWCNHs was about 1.8 times larger than that of pristine SWCNHs. The difference between "2 times" and "1.8 times" in the comparison using these different units suggests that oxidized SWCNHs can be packed more densely by compression than the pristine SWCNHs. This is due to the change in the structural flexibility of SWCNHs caused by mild oxidation, as is discussed in the next section.

Figure 10 shows the methane adsorption properties of SWCNHs prepared under the modified conditions (cathode-hole diameter = 12 mm; arc time = 70 s). Here, the micropores were opened on these SWCNHs by mild oxidation to burn-off values of 20% and 39%. In addition, these SWCNHs were compressed to apparent densities of 0.51 and 0.44 g cm^{-3}, respectively. In Fig. 10(a), it can be seen that the amount of methane adsorbed on these SWCNHs increased with increasing methane pressure, and the difference in this increase between these burn-off values was not significant. This means that these samples have almost the same capacity to adsorb methane even though they have different burn-off values. The reason for this result can be explained by the relationship between the burn-off and the micropore volume for SWCNHs prepared under the modified conditions, in which the micropore volume was not significantly different when the burn-off was raised from 20% to 40%, as mentioned in the preceding section.

Figure 10(b) shows a comparison of the amount of methane adsorbed on SWCNHs synthesized via conventional and modified synthetic conditions. In this comparison, the plots corresponding to the cases of the modified synthesis conditions exhibit larger amounts of adsorbed methane than that of the conventional condition at each apparent SWCNH density. Note that the amount of methane adsorbed on SWCNHs produced using the modified conditions with burn-offs of 20% and 39% increased by 36.4% and 48.7%, respectively, compared to those produced by the conventional condition. It is expected that the SWCNHs that exhibit higher methane adsorption properties should have larger micropore volumes. As mentioned in the explanation of Fig. 9(b), the micropore size distributions of the SWCNHs prepared using the modified conditions exhibited higher values than the SWCNHs prepared by the conventional synthetic condition, which is consistent with this expectation. The decrease of burn-off to 20% needed to achieve high methane adsorption is meaningful to reduce the loss of the net yield of adsorbent SWCNH.

The target that has been set for the practical use of storage media for adsorbents by the U.S. Department of Energy is 150 cm^3 cm^{-3}.[24] The SWCNHs produced via laser ablation reached 160 cm^3 cm^{-3} when they were oxidized and

compressed at 50 MPa.[24] The largest amount of methane adsorption on SWCNHs in the present study was 98.1 cm^3 cm^{-3}, which is lower than this target. Nevertheless, the maximum compression pressure used in this study was 18 MPa. The relationship of the compression pressure to the apparent SWCNH density shown in Fig. 8 suggests that the SWCNHs produced via the GI-AIW method seem to have a greater capacity to increase the apparent SWCNH density if the compression pressure is increased. Therefore, we believe that the amount of methane adsorbed on SWCNHs prepared in the manner described in this study will reach the target value if the compression pressure is increased. Further investigations on parameter variations, including the increase of the compression pressure, will be carried out in the future.

F. Effect of mild oxidation on the structural flexibility of SWCNHs

As mentioned above, it was revealed that the flexibility of SWCNHs was higher after mild oxidation treatment. In order to elucidate this effect, a molecular mechanics calculation[45,46] using a universal force field[45] was carried out on the horn model illustrated in Fig. 11. In this model, 78 C atoms were used to construct the pristine SWCNH unit. The commercial GAUSSIAN 03 W software was used to conduct the calculation. In order to evaluate the structural flexibility, the deformation energy, as defined by Eq. (2), was calculated.

$$\Delta E = E_1 - E_2 \tag{2}$$

In Eq. (2), ΔE, E_1, and E_2 are the deformation energy, the total energy of the SWCNH unit structure in the deformed structure, and the energy of the base structure, respectively. The deformed structure was determined by shrinking one radial axis, as shown in Fig. 11. In order to observe the effect of mild oxidation on the SWCNHs, we assume that three micropores are opened in this model by removing three atoms. Figure 11 shows the plots of the deformation energy of the SWCNH model against the extent of the deformation; the extent of deformation is expressed by the ratio of two radial axes (B/A). As seen in these plots, there is a tendency for the deformation energy of the porous SWCNH to be less than that for the pristine SWCNH. This result is qualitatively consistent with the experimental observations suggesting that the flexibility of porous SWCNHs is higher than that of pristine SWCNHs.

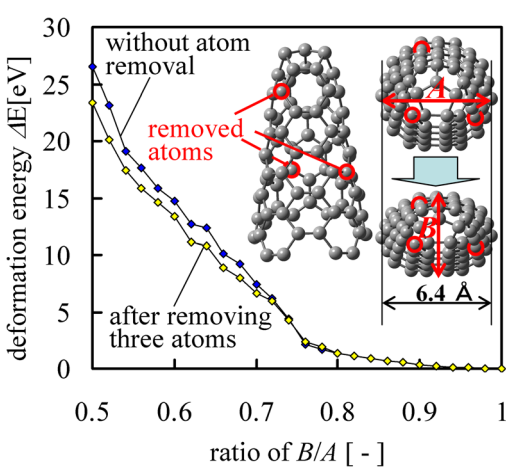

FIG. 11. (Color online) Deformation energy of SWCNHs calculated using a molecular mechanics calculation on the embedded SWCNH model. In order to observe the effect of mild oxidation on the SWCNH, three atoms are removed, representing pores generated by the oxidation.

IV. CONCLUSIONS

SWCNHs were synthesized via the GI-AIW method using a hollow graphite cathode. The diameter of the cathode hole was increased in order to control the consumption area of the graphite anode rod. As a result, the yield of the SWCNHs increased by six times. Due to this alteration of the electrode configuration, the structure of the as-grown SWCNHs changed remarkably; each horn in the aggregates became larger, and the thermal stability of the SWCNHs in an oxidative environment increased accordingly. An *ab initio* molecular orbital calculation was carried out in order to elucidate this phenomenon. When the conventional condition was applied, a burn-off of about 40% was necessary in order to achieve the maximum specific surface area and micropore volume. The burn-off required to reach the maximized values was reduced to almost half when the diameter of the cathode hole was increased. It was thought that the high micropore volume obtained from the larger cathode hole could enhance the methane adsorption. Accordingly, the SWCNHs obtained using the larger cathode hole exhibited a larger amount of adsorbed methane than did those obtained from the conventional synthetic condition. It was known that compression of powdery SWCNHs causes an increase of the amount of methane adsorbed per apparent volume of SWCNH bulk because the bulk density increases. It was found that this effect in oxidized SWCNHs was larger than in pristine SWCNHs. From this result, it was proposed that SWCNHs with micropores are more flexible than pristine SWCNHs. A molecular mechanics calculation supported the feasibility of this proposal.

Besides the cathode size and the arc duration time investigated here, one might consider that the structure, yield, and methane adsorption properties of the products obtained via the GI-AIW method could be further affected by the optimization of more factors, for example, the gas component, electrode motion, arc current control, and so forth, and thus further investigations will be carried out.

ACKNOWLEDGMENTS

This work is financially supported by a Japan Society for the Promotion of Science (JSPS) Grant-in-Aid for Exploratory Research (Contract No. 19656024), and by Scientific Research B Contract No. 21360394.

[1]S. Iijima, Nature **354**, 56 (1991).
[2]S. Iijima and T. Ichihashi, Nature **363**, 603 (1993).
[3]S. Iijima, M. Yudasaka, R. Yamada, S. Bandow, K. Suenaga, F. Kokai, and K. Takahashi, Chem. Phys. Lett. **309**, 165 (1999).
[4]N. Sano, H. Wang, M. Chhowalla, I. Alexandrou, and G. A. J. Amaratunga, Nature **414**, 506 (2001).
[5]A. Star and D. R. Kauffman, Angew. Chem. Int. Ed. **47**, 6550 (2008).
[6]D. Tasis, N. Tagmatarchis, A. Bianco, and M. Prato, Chem. Rev. **106**, 1105 (2006).

[7]R. Lu, J. J. Shi, F. J. Baca, and J. Z. Wu, J. Appl. Phys. **108**, 084305 (2010).
[8]Y. D. Guo, X. H. Yan, and Y. Xiao, J. Appl. Phys. **108**, 104309 (2010).
[9]J. Noh, M. Jung, K. Jung, S. Lim, G. Lee, V. Subramanian, A. D. Leonard, J. Tour, and G. Cho, J. Appl. Phys. **108**, 102811 (2010).
[10]Y. Yu, G. Song, and L. Sun, J. Appl. Phys. **108**, 084319 (2010).
[11]M. W. Cole, V. H. Crespi, M. S. Dresselhaus, G. Dresselhaus, J. E. Fischer, H. R. Gutierrez, K. Kojima, G. D. Mahan, A. M. Rao, J. O. Sofo, M. Tachibana, K. Wako, and Q. Xiong, J. Phys.: Condens. Matter. **22**, 334201 (2010).
[12]M. Endo, T. Hayashi, Y. A. Kim, and H. Muramatsu, Jpn. J. Appl. Phys. **45**, 4883 (2006).
[13]K. Hata, D. N. Futaba, K. Mizuno, T. Namai, M. Yumura, and S. Iijima, Science **306**, 1362 (2004).
[14]K. Hasegawa and S. Noda, Appl. Phys. Express **3**, 045103 (2010).
[15]S. Maghsoodi, A. Khodadadi, and Y. Mortazavi, Appl. Surf. Sci. **256**, 2769 (2010).
[16]M. Bystrzejewski, M. H. Ruemmeli, H. Lange, A. Huczko, P. Baranowski, T. Gemming, and T. Pichler, J. Nanosci. Nanotechnol. **8**, 6178 (2008).
[17]S. Scalese, V. Scuderi, S. Bagiante, F. Shimone, P. Russo, L. D'Urso, G. Compagnini, and V. Privitera, **107**, 014304 (2010).
[18]N. Sano, J. Phys. D: Appl. Phys. **37**, L17 (2004).
[19]N. Sano, J. Nakano, and T. Kanki, Carbon **42**, 686 (2004).
[20]T. Murakami, K. Ajima, J. Miyawaki, M. Yudasaka, S. Iijima, and K. Shiba, Mol. Pharm. **1**, 399 (2004).
[21]T. Yoshitake, Y. Shimakawa, S. Kuroshima, H. Kimura, T. Ichihashi, Y. Kubo, D. Kasuya, K. Takahashi, F. Kokai, M. Yudasaka, and S. Iijima, Physica B **323**, 124 (2002).
[22]N. Sano and S. Ukita, Mater. Chem. Phys. **99**, 447 (2006).
[23]K. Murata, J. Miyawaki, M. Yudasaka, S. Iijima, and K. Kaneko, Carbon **43**, 2826 (2005).
[24]E. Bekyarova, K. Murata, M. Yudasaka, D. Kasuya, S. Iijima, H. Tanaka, H. Kahoh, and K. Kaneko, J. Phys. Chem. B **107**, 4681 (2003).
[25]S. Utsumi, J. Miyawaki, H. Tanaka, Y. Hattori, T. Itoi, N. Ichikuni, H. Kanoh, M. Yudasaka, S. Iijima, and K. Kaneko, J. Phys. Chem. B **109**, 14319 (2005).
[26]E. Bekyarova, K. Kaneko, D. Kasuya, K. Murata, M. Yudasaka, and S. Iijima, Langmuir **18**, 4138 (2002).
[27]C. Poonjarernsilp, N. Sano, H. Tamon, and T. Charinpanitkul, J. Appl. Phys. **106**, 104315 (2009).
[28]H. Takikawa, M. Ikeda, K. Hirahara, Y. Hibi, Y. Tao, P. A. Ruiz, Jr., T. Sakakibarak, S. Itoh, and S. Iijima, Physica B **323**, 277 (2002).
[29]M. Ikeda, H. Takikawa, T. Tahara, Y. Fujimura, M. Kato, K. Tanaka, S. Itoh, and T. Sakakibara, Jpn. J. Appl. Phys. **41**, L852 (2002).
[30]T. Yamaguchi, S. Bandow, and S. Iijima, Chem. Phys. Lett. **389**, 181 (2004).
[31]M. Schiavon, U.S. Patent 7,**125**,525;EP 1428794 (2006).
[32]D. M. Gattia, M. V. Antisari, and R. Marazzi, Nanotechnol. **18**, 255604 (2007).
[33]N. Li, Z. Wang, K. Zhao, Z. Shi, Z. Gu, and S. Xu, Carbon **48**, 1580 (2010).
[34]N. Sano, T. Kikuchi, H. Wang, M. Chhowalla, and G. A. J. Amaratunga, Carbon **42**, 95 (2004).
[35]N. Sano, Y. Kimura, and T. Suzuki, J. Mater. Chem. **18**, 1555 (2008).
[36]T. Kawai, S. Okada, Y. Miyamoto, and A. Oshiyama, Phys. Rev. B **72**, 035428 (2005).
[37]D. Dollimore and G. R. Heal, J. Appl. Chem. **14**, 109 (1964).
[38]G. Horvath and K. Kawazoe, J. Chem. Eng. Jpn. **16**, 470 (1983).
[39]B. C. Lippens and J. H. de Boer, J. Catal. **4**, 319 (1965).
[40]N. Sano, T. Suzuki, K. Hirano, Y. Akita, and H. Tamon, Plasma Sources Sci. Technol. **20**, 034002 (2011).
[41]P. Byszewski, H. Lange, A. Huczko, and J. F. Behnke, J. Phys. Chem. Solids **58**, 1679 (1997).
[42]D. Kasuya and M. Yudasaka, New Diamond **73**, 2 (2004).
[43]W. J. Hehre, R. F. Stewart, and J. A. Pople, J. Chem. Phys. **51**, 2657 (1969).
[44]J. B. Foresman and A Frisch, *Exploring Chemistry with Electronic Structure Methods*, 2nd ed. (Gaussian, Pittsburgh, PA, 2003), pp. 13–37.
[45]A. K. Rappe, C. J. Casewit, K. S. Colwell, W. A. Goddard III, and W. M. Skiff, J. Am. Chem. Soc. **114**, 10024 (1992).
[46]Y. Li, N. Hu, G. Yamamoto, Z. Wang, T. Hashida, H. Asanuma, C. Dong, T. Okabe, M. Arai, and H. Fukunaga, Carbon **48**, 2934 (2010).